EFFECTS OF CONTACT PRESSURE AND INTERFACE TEMPERATURE ON THERMAL CONTACT RESISTANCE BETWEEN 2Cr12NiMoWV/BH137 AND γ-TiAl/2Cr12NiMoWV INTERFACES

by

Yuwei LIU[a*], Yameng JI[b], Fuhao YE[c], Weizheng ZHANG[b*], and Shujun ZHOU[a]

[a] School of Mechanical Electronic and Information Engineering, China University of Mining and Technology, Beijing, China
[b] School of Mechanical Engineering, Beijing Institute of Technology, Beijing, China
[c] Huawei Machine Co., Ltd., Dongguan, China

Original scientific paper
https://doi.org/10.2298/TSCI191018470L

Thermal contact resistance between interfaces is an important parameter in the analysis of temperature distribution for structural components. Thermal contact resistance between heat resistant steel 2Cr12NiMoWV/aluminum alloy BH137 interfaces and 2Cr12NiMoWV/titanium alloy γ-TiAl interfaces were experimentally investigated in the present paper. The effects of contact pressure and interface temperature were detailed. The temperature of contacting surfaces was from 80-250 ℃, and the contact pressure ranged from 2-17 MPa. All experiments were conducted in ambient atmosphere. Results showed that thermal contact resistance decreases with an increment of interface temperature or contact pressure. Under the same conditions of contact pressure and interface temperature, thermal contact resistance between 2Cr12NiMoWV and BH137 interfaces is lower than that between 2Cr12NiMoWV and γ-TiAl interfaces. The temperature dependence of thermal conductivity and mechanical properties was analyzed to explain the results. Furthermore, with the piston and piston pin as the research object, steady state temperature fields were simulated in cases of considering thermal contact resistance and without considering thermal contact resistance, respectively. The results showed that the maximum temperature of the piston pin will be lower when thermal contact resistance is considered.

Key words: *thermal contact resistance, contact pressure, interface temperature, temperature distribution, piston*

Introduction

Contact heat transfer is important in many engineering applications such as automobiles, aircrafts, and turbines. Their working performances are highly influenced by the heat transfer between the contacting surfaces, and the primary factor limiting the heat transfer along the conduction paths is the thermal contact resistance (TCR), which is the reciprocal of thermal contact conductance (TCC). The TCR can be applied to help obtain an accurate characterization of heat-flows across interfaces in contact, which is essential for the analysis of temperature field and structural design of high temperature components.

* Corresponding authors, e-mails: yuweiliu1@126.com, zhangwz@bit.edu.cn

Engineering surfaces of solids are rough on the microscale and contacts occur only between the higher asperities. As a consequence the real contact area takes a quite small fraction (1-2 % for metallic contact) of the nominal contact area, and most of the heat-flowing through the actual contact spots is restricted by an effective TCR between the surfaces, which causes the *bulk temperature* at the interface or on a plane slightly below the interface to differ between the two contacting bodies [1]. There exist a wide range of factors that may influence TCR/TCC such as material properties, contact pressure, interface temperature, roughness, surface oxidation, heat-flow direction, contact pressure overloading, and load cycling [2, 3]. Numerous analytical and experimental studies have been conducted to determine TCR based on surface topography, elastic-plastic deformation, fractal theory, and so on. An early analysis of a thermal contact on an idealized shape of contact was carried out by Fenech and Rohsenow [4]. Cooper *et al.* [5] established the earliest plastic model which has been named as CMY model, showing reasonable predictions at room temperature. Mikic [6] proposed a TCR model considering elastic and plastic deformation of the micro contact spots. Subsequently, considerable numbers of researchers [7-9] developed TCR model for fractal surfaces by applying the Cooper-Mikic-Yovanovich (CMY) model or its modified forms. A power exponent relation was established between the TCC and the contact pressure. A similar conclusion can be found in [10]. Yovanovich [11] extensively reviewed the articles focusing research on the effects of TCC and highlighted that various conductance models should be *examined experimentally*. Bi *et al*. [12] pointed out that the relationship between the TCC and the contact pressure is nearly liner through studying the effects of interface temperature, contact pressure and material on TCC at temperatures in the range of 70 K to 290 K and pressures of 0.2 MPa to 0.7 MPa. Their results were consistent with later researches [13, 14]. Fieberg and Kneer [15] proposed an experimental approach to derive TCR according to contact heat transfer coefficients under high temperature and high pressure conditions. They found that TCC is proportional to the contact pressure and the effect of the temperature should not be neglected. High temperature under different interface conditions was experimentally investigated by Liu *et al*. [16]. The results showed that TCR decreases with the increment of the interface temperature. Apart from interface temperature and contact pressure, experimental and analytical studies were presented by [2, 17-19] to study the effect of specimen surface roughness on TCR. Their findings revealed that rough surfaces exhibit higher TCR under the same conditions [20]. The changes in the hardness as well as the thermal conductivity of the contacting body affect the TCC, for example see [21-23]. Their research results indicated that the material with lower yield strength or hardness value and high thermal conductivity shows better improvement in TCC.

Aluminum alloy, BH137, titanium alloy, γ-TiAl, and heat-resistant steel, 2Cr12NiMoWV are widely applied in high pressure temperature components. Many critical parts, such as pistons, bearings, clutches, pumps, *etc*., are made of these materials. The study on the TCR of γ-TiAl/2Cr12NiMoWV interfaces and 2Cr12NiMoWV/BH137 interfaces plays an important role in the structural design of engines and other critical component, but few studies concerning this topic has been done for these three materials. In this paper, the effects of the contact pressure (2-17 MPa) and interface temperature (80-250 °C) on TCR between these materials were investigated. And the temperature dependent mechanical and thermal properties are used to explain the results. Taking into consideration the measured TCR, numerical calculation is proceeded to obtain a more accurate temperature field of a diesel piston and piston pin.

Experimental approach

Test principle

The TCR is calculated by dividing the temperature drop to the average heat flux at the interface of contacting bodies, *i. e.* using eq. (1) [24]:

$$R = \frac{\Delta T}{q} \tag{1}$$

where R is the TCR, q [Wm^{-2}] – the average heat flux through the contact, and ΔT [°C] – the temperature drop at the interfaces due to imperfect contact.

The steady-state method is adopted in this paper and under the prediction of 1-D heat transfer, the temperature drop, ΔT, can be calculated by extrapolating the temperature at the location of the sensors to the interfaces.

The heat flux can be obtained according to the Fourier law:

$$q = -\lambda \frac{\mathrm{d}T}{\mathrm{d}x} \tag{2}$$

where λ is the thermal conductivity and the variation of thermal conductivity plays an important role in the calculation of TCR [21]. In this paper, the authors follow the technique used by Tang, and Zhang [14] to deal with the variation of thermal conductivity with temperature. Although relation of the thermal conductivity and the temperature is commonly non-linear, if the change is small, a linear relationship between them can be assumed:

$$\lambda(T) = \lambda_0 \left(1 + \frac{T}{m} \right) \tag{3}$$

where $\lambda(T)$ is the thermal conductivity at temperature T, λ_0, and m are constants. Substituting eq. (3) into eq. (2) yields the following equation for the heat flux:

$$q = \frac{T_i - T_j}{\delta} \lambda_0 \left[1 + \frac{1}{2m} (T_i + T_j) \right] \tag{4}$$

where T_i and T_j are the temperatures of the test points, and δ is the corresponding distance.

Test materials

The materials measured were aluminum alloy, heat resistant steel, and titanium alloy. Material properties tended to change with temperature, and this should be taken into consideration in the calculation of TCR. Figures 1 and 2 showed the thermal conductivities and yield strengths of BH137, 2Cr12NiMoWV, and γ-TiAl under various temperatures, respectively. As can be seen in fig. 1, the thermal conductivity of BH137 obvious increases as the temperature rises and is significantly greater than that of the other two materials. The effects of the temperature are not remarkable to 2Cr12NiMoWV and γ-TiAl. In the following fig. 2, yield strengths of both BH137 and 2Cr12NiMoWV decrease with increase of temperature. While, the yield strength of γ-TiAl drops slightly with the temperature increasing. The yield strength of BH137 is the least among three kinds of these materials.

Experimental facility

Standard ASTM D 5470 was referred to in this study for the test procedure and data processing. A brief description was given further in the text. The device consisted of five sub-

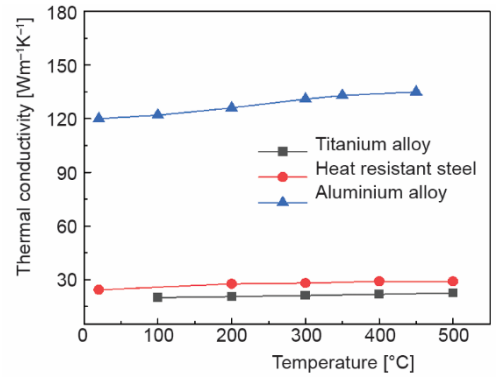

Figure 1. Variation of thermal conductivity with temperature for different materials

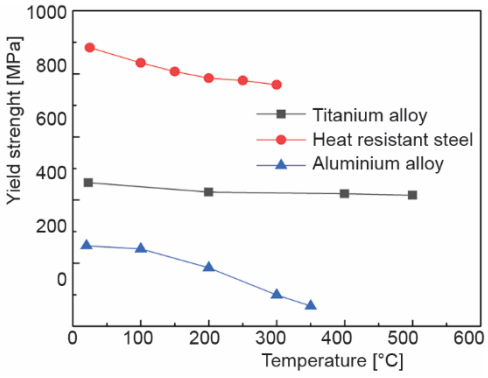

Figure 2. Variation of yield strength with temperature for different materials

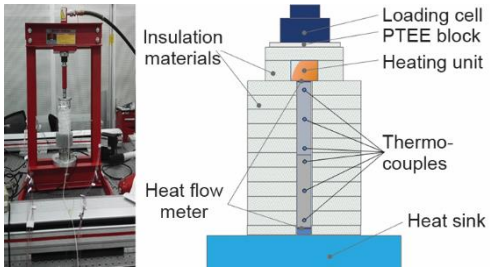

Figure 3. Schematic of TCR test system

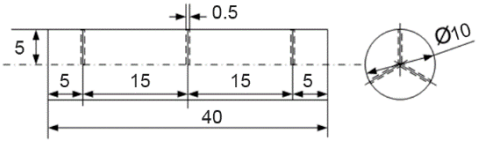

Figure 4. Sketch of test specimen [mm]

systems: heating sub-system, heat preservation sub-system, cooling sub-system, loading sub-system, and temperature sub-system, as shown in fig. 3. The specimens of cylindrical shape with diameter 10 mm and length 40 mm had been placed in contact, and the surface roughness was Ra = 1.6. In order to obtain a downward axial heat-flow, the ends of those two specimens were heated from the upper side and cooled from the lower side. Therefore, the heat sequentially flowed through the upper specimen, the contact interface, and the lower specimen from the top down. On top of the upper specimen was the heater controlled by a thermostat, on which a loading cell was assembled. The insulating materials were used in the prevention of heat dissipation from the radial direction. The temperatures at different axial locations of the two specimens were measured in atmospheric environment with T-type thermocouples. Three thermocouple positions were selected for each specimen along axial direction and the distance between the adjacent positions was 15 mm, as shown in fig. 4. For each axial position, three holes of diameter 0.5 mm and depth of 5 mm were evenly drilled along circumference to insert thermocouples. Each test was repeated more than five times and the mean was taken to eradicate any discrepancies. The tolerance at repeatability was around 3.6%.

Error analysis

The error caused of the experimental device can be quantitatively analyzed by using the method of comprehensive uncertainty analysis. Error sources, listed in tab. 1, are independent of one another and reveal normal distribution. According to the theory of error propagation law [18], the overall uncertainty for the estimation of TCR can be expressed in eq. (5):

$$e_{\max} = \sqrt{e_1^2 + e_2^2 + \ldots + e_{n-1}^2 + e_n^2} \tag{5}$$

where e_i, $i = 1 \ldots n$.

The position error caused by the thermocouple installed in the test hole of the specimen has little effect on the measurement of temperature. For materials with higher thermal conductivities, the error formed on the length of ±15 μm is much smaller than 0.001 °C and its effect on TCR can be ignored.

The error of pressure sensor mainly affects the test result under the current test pressure. Assuming that TCR varies linearly within a minute pressure fluctuation, the maximum error, e_1, caused by the pressure sensor in measurement system should be ±0.2%.

Table 1. Sources of experimental errors

Error source	Uncertainty
Temperature calibration error	±0.003 °C
Position error of temperature sensor	±15 μm
Pressure sensor error	±0.2%
Area error	±0.08%
Heat leakage error	max: 2.4%
Heat meter measurement error	±5%

Area error refers to the error of the contact area due to the processing error. The influence of area error on TCR is mainly related to the heat flux through the interface, which has positive correlation with the reciprocal of the area. Based on the error transfer function, the error, e_2, due to the area error defined by eq. (6) is around 0.08%, indicating that this error is negligible:

$$\left(\frac{1}{1+0.08\%}-1\right)<e_2<\left(\frac{1}{1-0.08\%}-1\right) \tag{6}$$

Heat dissipates through the insulation material in the atmosphere and the error of heat leakage is ±2.4%. The error, e_3, caused by heat leakage error acting on TCR can be obtained by eq. (7), which ranges from 2.34% to 2.46%:

$$\left(\frac{1}{1+2.4\%}-1\right)<e_3<\left(\frac{1}{1-2.4\%}-1\right) \tag{7}$$

The test error of the heat-flow meter is ±5%, resulting in that the addition error of TCR, e_4, changes from 4.76% to 5.26%:

$$\left(\frac{1}{1+5\%}-1\right)<e_4<\left(\frac{1}{1-5\%}-1\right) \tag{8}$$

Substituting each error into eq. (5), the total maximum uncertainty in measured TCR is 5.81%.

Results and discussion

Test arrangement

The effects of contact pressure and contact interface temperature on TCR between 2Cr12NiMoWV/BH137 interfaces and γ-TiAl/2Cr12NiMoWV interfaces were studied. According to the working conditions of a diesel piston, the interface temperature varied between 80-250 °C, and the contact pressure ranged from 2-17 MPa. Figure 5 lists the detailed conditions.

Data processing

Ideally, heat transferred from top to bottom and flowed into upper test piece, contact interface, lower test piece, heat sink in turn, which formed a complete 1-D heat conduction path.

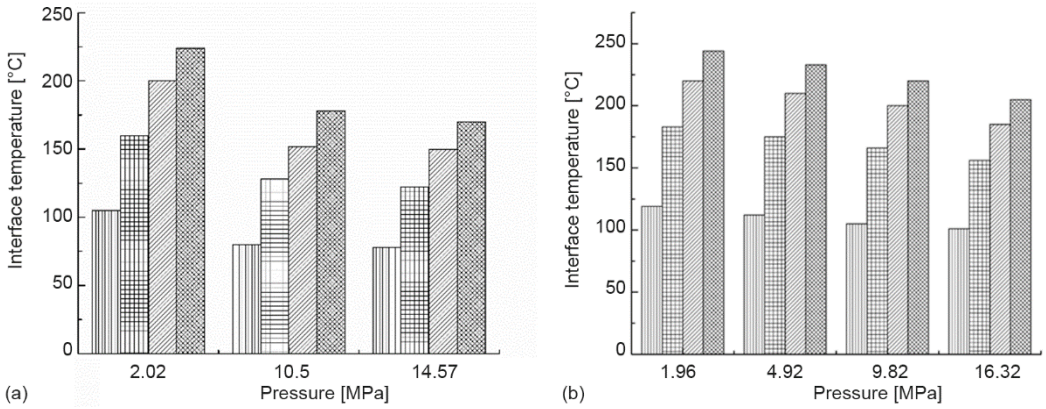

Figure 5. Pressure and Interface temperature conditions; (a) experimental conditions for 2Cr12NiMoWV/BH137 contacts, (b) experimental conditions for γ-TiAl/2Cr12NiMoWV contacts

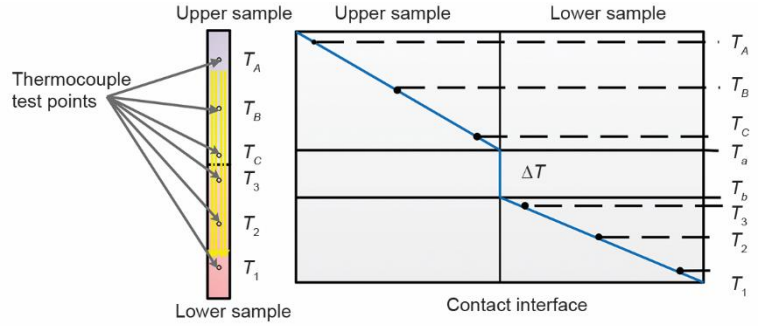

Figure 6. Positions of test points on the ideal heat transfer path

Table 2. Sources of experimental errors

State time	Stage-1	Stage-2	Stage-3	Stage-4
Heater power [W]	6.30	11.56	14.94	18.55
Interface temperature [°C]	80	128	152	178
Thermal contact resistance [°CW^{-1}]	1.06	0.90	0.74	0.61

The effective temperatures of the test points from top to bottom on the test pieces were, in order, T_A, T_B, T_C, T_3, T_2, and T_1, shown in fig. 6. Each one was the arithmetic average value of the records of thermocouples at the same position. The T_a and T_b denoted temperatures at the top and bottom interface, respectively, which could not be directly monitored by a thermocouple. They were inferred from the effective temperatures of the test points and thereby the temperature difference between the upper and lower interfaces was obtained. The TCR at the interface was calculated by substituting the known temperature difference and the heat flux measured by the heat meter into eq. (1). For example, under the contact pressure of 10.5 MPa, the temperatures of test points with time for 2Cr12NiMoWV/BH137 interfaces were shown in fig. 7. The corresponding interface temperatures and TCR were listed in tab. 2.

Influence of interface temperature

All of the curves in fig. 8 indicate that TCR decreases with the increment of the interface temperature at a constant contact pressure, which may result from the following reasons:

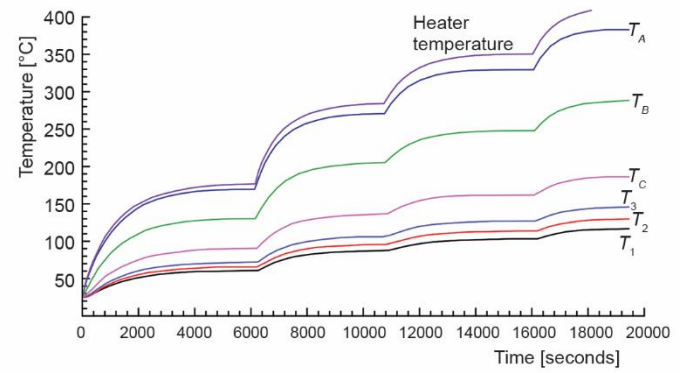

Figure 7. The curves of temperatures of test points varying with time

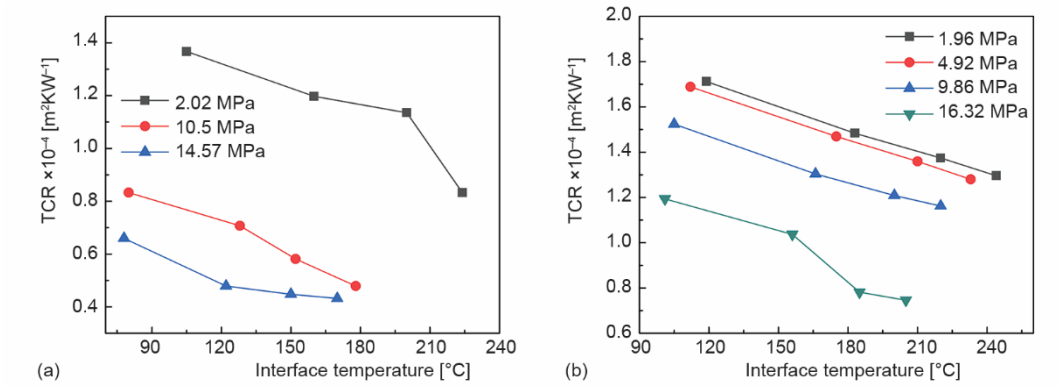

Figure 8. Effect of interface temperature on TCR; (a) TCR for 2Cr12NiMoWV/ BH137 contacts, (b) TCR for γ-TiAl/2Cr12NiMoWV contacts

First, the yield strength of the contact materials, fig. 2, decreases with the increasing interface temperatures, enlarging the real contact area at the same contact pressure. Second, the interface radiation heat transfer may influence reduction in the contact resistance, although the interface radiation effect is very limited when the interface temperature is less than 850 K (580 °C) [25]. Third, all the experiments were carried out under atmospheric condition, so the contact surface of specimens would contain air. The conductivity of air increases with increasing temperature, causing increases in interface gas conduction [2]. Fourth, the temperature-dependent TCR is in inverse ratio to the temperature-dependent thermal conductivity of the materials [26].

For BH137/2Cr12NiMoWV interfaces, presented in fig. 8(a), under a low contact pressure of 2.02 MPa, the interface TCR descends evidently from 1.37×10^{-4} m^{2}K/W to 8.33×10^{-5} m^{2}K/W when the interface temperature increases from 105-224 °C, leading to a 39.14% decline. While, the interface temperature ranging between 122 °C to 173 °C contributes to a 9.81% drop in TCR under a higher contact pressure of 14.57 MPa. This is mainly because the aluminum alloy BH137 has a lower yield strength than the heat resistant steel 2Cr12NiMoWV and the difference between these two materials is relatively large. The hardness of aluminum alloy is sensitive to contact pressure variety [27] and the clearance of the contact interface will be larger at the lower contact pressure, resulting in more radiation heat exchange. Along with the contact pressure increases, solid conduction through contacting solid spots is

gaining dominance and the effect of interface temperature becomes comparatively smaller. It is shown from fig. 8(b) that when the interface temperature increases from 101-244 °C, the reduction levels of TCR under the contact pressure of 1.96 MPa, 4.92 MPa, 9.86 MPa, and 16.32 MPa are 24.30%, 24.21%, 23.75%, and 37.52%, respectively.

Influence of contact pressure

Figure 9 illustrates that increases in contact pressure enhance contact heat transfer. It is observed from fig. 9(a) that, at the interface temperature of 88 °C, as the contact pressure increases from 2.02 MPa to 14.57 MPa, the interface TCR value decreases from 1.37×10^{-4} m^2K/W to 0.66×10^{-4} m^2K/W. At the interface temperature of 191 °C, it decreases from 8.36×10^{-5} m^2K/W to 4.32×10^{-5} m^2K/W. The former has a bigger decline of 51.80% compared with the latter of 47.10%. This is because contact pressure directly affects the deformation of the contact surfaces causing more asperities into contact, resulting in that the real contact area is more enhanced, and so is the solid heat transfer. However, under the contact pressure of 14.57 MPa, there are only small differences for the results with the interface temperature ranging from 137-191 °C. The value of TCR changes a little and tends to be stable under the relative high contact pressure and high interface temperature. This may be caused by the fact that the real contact area will be slightly influenced by the contact pressure once the real contact area increases to a certain extent. In fig. 9(b), when the changing range of the contact pressure is from 1.96-16.32 MPa, the interface TCR value has a 30.3% decline and decreases from 1.71×10^{-4} m^2K/W to 1.20×10^{-4} m^2K/W at the interface temperature of 109 °C. While its TCR drop is 42.4% at 226 °C of the interface temperature. Figure 9(b) presents that the variation tendencies of the TCR values against contact pressure are similar at different interface temperatures, the drop of TCR is more significant when the contact pressure is higher than about 10 MPa. This may be explained by the higher yield strength of γ-TiAl and 2Cr12NiMoWV compared to that of BH137, and by that the asperities on the contacting surfaces are more likely to experience elastic-plastic deformation. Larger deformation will occur under high contact pressure, resulting in a greater reduction in the TCR value.

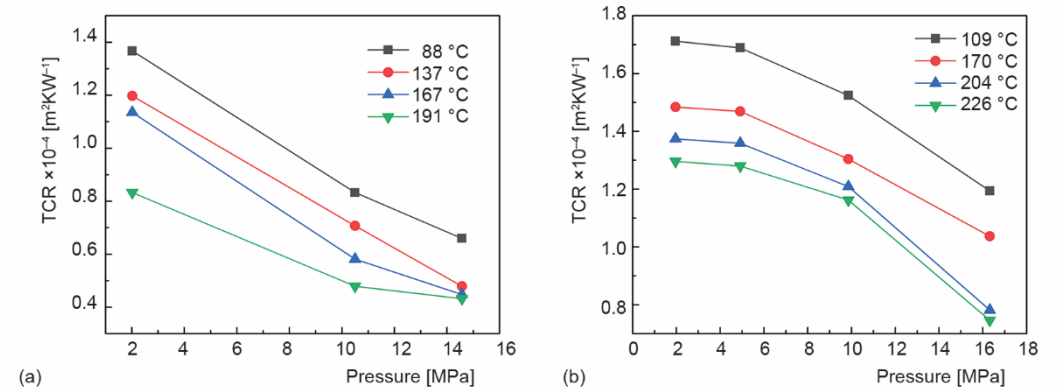

Figure 9. Effect of contact pressure on TCR; (a) TCR for 2Cr12NiMoWV/ BH137 contacts, (b) TCR for γ-TiAl/2Cr12NiMoWV contacts

In addition, under the same conditions of contact pressure and interface temperature, TCR between γ-TiAl and 2Cr12NiMoWV is larger than that between 2Cr12NiMoWV/BH137.

For instance, when the interface temperature is 165 °C and the contact pressure is 10.0 MPa, the value of TCR is 1.662×10^{-4} m^{2}K/W for γ-TiAl/2Cr12NiMoWV interfaces and is 6.750×10^{-5} m^{2}K/W for 2Cr12NiMoWV/BH137 interfaces, respectively. The changes of thermal conductivity and yield strength of each material are diverse at different temperature, which have been illustrated in figs. 1 and 2, and they are the influence factors to TCR.

Thermal analysis of the piston and piston pin

The research findings mentioned above supply the reliable assurance for material selection and temperature distribution calculation of a diesel piston pin. The piston was made of heat-resistant steel and an important design objective of this piston was to block heat transferring into the piston pin. The value of TCR between 2Cr12NiMoWV/BH137 interfaces was lower than that of γ-TiAl/2Cr12NiMoWV interfaces. Therefore, BH137 was selected as the material of the piston pin. At the same time, in order to accurately obtain the temperature field of the piston pin, numerical results were compared according to whether TCR was taken into account or not. The value of TCR between 2Cr12NiMoWV and γ-TiAl contact surfaces was determined based on the above experimental results. Their thermal physical parameters are listed in tabs. 3 and 4, respectively. The interior of the piston does not produce heat itself and the heat mainly originates from the hot gas in the combustion chamber. The gas has a high temperature, and convection heat transfer occurs between the gas and the top surface of the piston. Therefore, thermal analysis in the piston can be treated as a steady-state analysis, which has no inner heat source. Accurate heat transfer boundary condition is a crucial part in temperature prediction of the piston. For a four-stroke internal combustion engine, the average heat transfer coefficient, h_{gm}, and gas temperature, T_{gm}, on the top surface of the piston can be defined by eqs. (9) and (10) [28]:

$$h_{gm} = \frac{1}{4\pi}\int_0^{4\pi} h_g \mathrm{d}\theta \tag{9}$$

$$T_{gm} = \frac{1}{4\pi h_{gm}}\int_0^{4\pi} T_g h_g \mathrm{d}\theta \tag{10}$$

where h_g is the transient heat transfer coefficient, T_g – the transient gas temperature, θ – the crank angle. According to the bench test data, the characters of the engine were calculated using RICARDO-WAVE software, and then the trends of the transient heat transfer coefficient and the transient gas temperature with the change in crank angle were obtained. In addition, the heat transfer coefficients and environmental temperatures of the rest of the fields which include the

Table 3. Material properties of 2Cr12NiMoWV

Temperature [°C]	20	200	300	400	500	600
Thermal conductivity [Wm^{-1}K^{-1}]	24.3	27.7	28.1	29.1	29.1	29.7
Coefficient of linear expansion [10^{-6}°C^{-1}]	10.38	10.82	11.21	11.49	11.82	12.06
Specific heat [Jg^{-1}°C^{-1}]	530	585	627	663	721	860
Elastic modulus [GPa]	216	205	198	189	178	
Density [gcm^{-3}]	7.84					

Table 4. Material properties of γ-TiAl

Temperature [°C]	20	200	300	400	500	600
Thermal conductivity [$Wm^{-1}K^{-1}$]	20.6	21.2	21.9	22.6	23.3	24.1
Coefficient of linear expansion [$10^{-6}°C^{-1}$]	8.47	9.76	10.60	11.4	11.80	12.00
Specific heat [$Jg^{-1}°C^{-1}$]	742	745	748	750	751	752
Elastic modulus [GPa]	172	168	166	161	157	154
Density [gcm^{-3}]	3.87					

ring grooves, piston lands, piston skirt and the piston pin were calculated separately. By referring to [29], the temperature and heat transfer coefficient were applied on finite element model as third boundary condition and the temperature field was calculated.

As the piston and piston pin were symmetrical in structure, 1/2 scale model was used in this study to promote calculation efficiency. The ABAQUS finite element package [30] was utilized in this study to provide a convenient tool for the temperature field of the model. There are two basic types of contact used in ABAQUS software: node-to-surface contact, and surface-to-surface contact. Surface-to-surface contact is the most common type of contact used for bodies that have arbitrary shapes with relative large contact areas [31]. Surface-to-surface contact was the type of contact between the piston pin hole and the piston pin assumed in this analysis. The piston model was simplified by the small transition radii and edge chamfering before the grid division of the computational model. The mesh was constructed using three-dimensional continuum elements from the ABAQUS/Standard library, consisting of heat transfer 4 node solid elements DC3D4. The mesh convergence study was carried out to guarantee the requirements that the relative temperature error was less than 5%. The final simulation model included 67,317 whole nodes and 335,843 elements, shown in fig. 10.

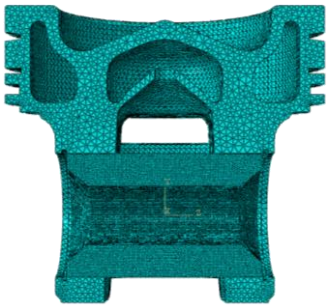

Figure 10. Finite element model of piston and piston pin

Figures 11 and 12 show the temperature distributions of the piston pin by considering TCR or not, respectively. By contrast, it can be seen that the maximum temperature in fig. 11 is about 6 °C lower than that of fig. 12. It is necessary to take into account the effect of TCR to achieve a more accurate temperature distribution, which relates to the thermal structure design.

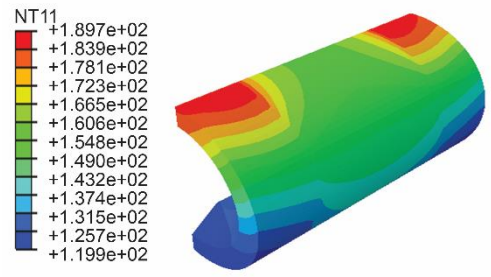

Figure 11. Whole temperature field considering TCR

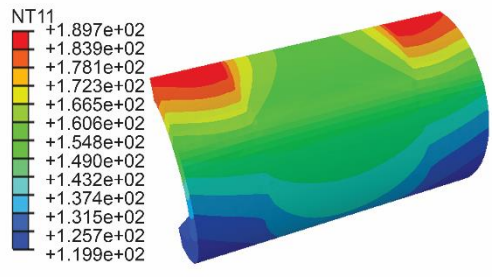

Figure 12. Whole temperature field without considering TCR

Conclusions

The TCR was experimentally measured in the atmospheric environment. Contact resistances between aluminum alloy BH137/heat-resistant steel 2Cr12NiMoWV surfaces, and heat-resistant steel 2Cr12NiMoWV/titanium alloy γ-TiAl surfaces were measured at various interface temperature and contact pressure. Results reveal the following.

- The TCR decreases with an increment of interface temperature or contact pressure. The material with lower yield strength and high thermal conductivity contributes to a lower TCR.
- Under the same conditions of contact pressure and interface temperature, the value of TCR between BH137 and 2Cr12NiMoWV interfaces is better than that between 2Cr12NiMoWV and γ-TiAl interfaces.
- The temperature field of a piston and piston pin was simulated by considering TCR or not. The maximum temperature of the piston pin with TCR decreases about 6 °C. The effect of TCR should be taken into account to guarantee a more accurate temperature distribution.

We suggest conducting further experimental studies under wider ranges of interface temperature and contact pressure, and conducting a model to predict the TCR satisfactorily.

Acknowledgement

This paper was partially supported by the National Natural Science Foundation of China grant 51804313 and by the Tribology Science Foundation of State Key Laboratory of Tribology Tsinghua University (SKLTKF18B06).

References

[1] Roberts, N. A., Walker, D. G., A Review Of Thermal Rectification Observations and Models in Solid Materials, *International Journal of Thermal Sciences, 50* (2011), 5, pp. 648-662
[2] Dou, R., *et al.*, Effects of Contact Pressure, Interface Temperature, and Surface Roughness on Thermal Contact Conductance between Stainless Steel Surfaces under Atmosphere Condition, *International Journal of Heat and Mass Transfer, 94* (2016), Mar., pp. 156-163
[3] Zhao, Z., *et al.*, Effects of Pressure and Temperature on Thermal Contact Resistance between Different Materials, *Thermal Science, 19* (2015), 4, pp. 1369-1372
[4] Fenech, H., Rohsenow, W. M., Prediction of Thermal Conductance of Metallic Surfaces in Contact, *Journal of Heat Transfer, 85* (1963), 1, pp. 15-24
[5] Cooper, M., *et al.,* Thermal Contact Conductance, *International Journal of Heat & Mass Transfer, 12* (1969), 3, pp. 279-300
[6] Mikic, B. B., Thermal Contact Conductance: Theoretical Considerations, *International Journal of Heat & Mass Transfer, 17* (1974), 2, pp. 205-14
[7] Sadowski, P., Stupkiewicz, S., A Model of Thermal Contact Conductance at High Real Contact Area Fractions, *Wear, 268* (2010), 1-2, pp. 77-85
[8] Patil, D. B., Eriten, M., Effects of Interfacial Strength and Roughness on the Static Friction Coefficient, *Tribology Letters, 56* (2014), 2, pp. 355-374
[9] Zhang, J., *et al.*, A Fractal Model for Predicting Thermal Contact Conductance Considering Elasto-Plastic Deformation and Base Thermal Resistances, *Journal of Mechanical Science and Technology, 33* (2019), 1, pp. 475-484
[10] Xing, L., *et al.*, Experimental Investigation of Contact Heat Transfer at High Temperature Based on Steady-State Heat Flux Method, *Experimental Heat Transfer, 23* (2010), 2, pp. 107-116
[11] Yovanovich, M. M., Four Decades of Research on Thermal Contact, Gap, and Joint Resistance in Microelectronics, *IEEE Transactions on Components & Packaging Technologies, 28* (2005), 2, pp. 182-206
[12] Bi, D., *et al.,* Influences of Temperature and Contact Pressure on Thermal Contact Resistance at Interfaces at Cryogenic Temperatures, Cryogenics, 52 (2012), 7-9, pp. 403-409
[13] Chen, J., *et al.*, Determination of Thermal Contact Conductance between thin Metal Sheets of Battery Tabs, *International Journal of Heat and Mass Transfer, 69* (2014), Feb., pp. 473-480

[14] Tang, Q., Zhang, W., The Effect of Pressure on Thermal Contact Conductance of Superalloys under High Temperature, *International Journal of Heat and Mass Transfer, 103* (2016), Dec., pp. 1208-1213
[15] Fieberg, C., Kneer, R., Determination of Thermal Contact Resistance from Transient Temperature Measurements, *International Journal of Heat & Mass Transfer, 51* (2008), 5-, pp. 1017-1023
[16] Liu, D., *et al.,* Experimental Investigation of High Temperature Thermal Contact Resistance between High Thermal Conductivity C/C Material and Inconel 600, *International Journal of Heat and Mass Transfer, 80* (2015), Jan. pp. 407-410
[17] Oh, J. H., *et al.,* Phonon Thermal Conductivity in Silicon Nanowires: The Effects of Surface Roughness at Low Temperatures, *Journal of Applied Physics, 111* (2012), 4, 044304
[18] Chen, Y., Zhang, C., Role of Surface Roughness on Thermal Conductance at Liquid-Solid Interfaces, *International Journal of Heat and Mass Transfer, 78* (2014), Nov., pp. 624-629
[19] Zheng, J., *et al.*, Measurements of Interfacial Thermal Contact Conductance between Pressed Alloys at Low Temperatures, *Cryogenics, 80* (2016), Dec., pp. 33-43
[20] Akinyemi, O. D., Sauer, T., Effects of Heat Sink Compounds on Contact Resistance of Porous Media, *Thermal Science, 11* (2007), 4, pp. 113-124
[21] Gopal, V., *et al.*, Thermal Contact Conductance and its Dependence on Load Cycling, *International Journal of Heat and Mass Transfer, 66* (2013), Nov., pp. 444-450
[22] Tang, Q., *et al.,* Influencing Factors of Thermal Contact Conductance between TC4/30CrMnSi Interfaces, *International Journal of Heat and Mass Transfer, 86* (2015), Jul., pp. 694-698
[23] Tariq, A., Asif, M., Experimental Investigation of Thermal Contact Conductance for Nominally Flat Metallic Contact, *Heat and Mass Transfer, 52* (2016), 2, pp. 291-307
[24] Zhang, P., *et al.,* A High-Precision Instrumentation of Measuring Thermal Contact Resistance using Reversible Heat Flux, *Experimental Thermal and Fluid Science, 54* (2014), 2, pp. 204-211
[25] Liu, D. H., Shang, X. C., The Physical-Mechanism Based High-Temperature Thermal Contact Conductance Model with Experimental Verification, *Chinese Physics Letters, 30* (2013), 3, 036501
[26] Zheng, J., *et al.*, Measurements of Interfacial Thermal Contact Conductance between Pressed Alloys at Low Temperatures, *Cryogenics, 80* (2016), Dec., pp. 33-43
[27] Bahrami, M., *et al.,* Modeling Thermal Contact Resistance: A Scale Analysis Approach, *J. Heat Transfer, 126* (2004), 6, pp. 2004-2016
[28] Annand, W. J., Heat Transfer in the Cylinders of Reciprocating Internal Combustion Engines, *Proc. Inst. Mech. Engrs., 177* (1963), 1, pp. 973-990
[29] Gao, Y. F., The Structure Design of Titanium Alloy Lightweight Piston, Ph. D. thesis, Beijing: Beijing Institute of Technology, Beijing, 2016, pp. 26-33
[30] ***, ABAQUS Theory Manual, Version 6.13, Simulia INC, 2013
[31] Abdullah, O. I., Schlattmann, J., Temperature Analysis of a Pin-on-Disc Tribology Test using Experimental and Numerical Approaches, *Friction, 4* (2016), 2, pp. 135-143

Paper submitted: October 18, 2019
Paper revised: December 4, 2019
Paper accepted: December 8, 2019